Proof of scale invariant solutions in the Kardar–Parisi–Zhang and Kuramoto–Sivashinsky equations in 1+1 dimensions: analytical and numerical results

Victor S L'vov†‡, Vladimir V Lebedev†§, Miriam Paton‖ and Itamar Procaccia‖

† Department of Nuclear Physics, The Weizmann Institute of Science, Rehovot 76100, Israel
‡ Institute of Automation, Academy of Sciences of Russia, Novosibirsk, 630090 Russia
§ Landau Institute for Theoretical Physics, Academy of Sciences of Russia, 117940, GSP-1, V-334, Kosygina 2, Moscow, Russia
‖ Department of Chemical Physics, The Weizmann Institute of Science, Rehovot 76100, Israel

Abstract. Under the *assumption* that the Kardar–Parisi–Zhang (KPZ) model possesses scale invariant solutions, there exists an exact calculation of the dynamic scaling exponent $z = 3/2$. In this paper we *prove* that both KPZ and the related Kuramoto–Sivashinsky (KS) model indeed possess scale invariant solutions in 1+1 dimensions which are in fact the same for both models. The proof entails an examination of the higher order diagrams in the perturbation theory in terms of the dressed Green function and the correlator. Although each higher order diagram contains logarithmic divergences, endangering the existence of the scale invariant solution, we show that these divergences cancel in each order. The proof uses a fluctuation–dissipation theorem (FDT), which is an exact result for KPZ in 1+1 dimensions. Since we prove that there are no divergences, all the diagrams are dominated by local interactions in k-space. This local-in-k solution of the KPZ equation is also the solution of the KS equation, because the two equations have the same nonlinearity, and the nonlinear term dominates in the long-wavelength regime when $z = 3/2 < 2$. Consequently we discover that KPZ and KS are equivalent in 1+1 dimensions, contrary to their behaviour in 2+1 dimensions. Our analytical results are supplemented with extensive numerical simulations of the KS equation. It is shown that in accordance with the analytical results the statistics of the simultaneous fluctuations in KS are Gaussian, and that the dynamic exponent is $z = 3/2$.

PACS numbers: 0540, 6150C.

1. Introduction

1.1. Equations of motion

Dynamical surface roughening occurs in a variety of physical contexts, like flame propagation, growth of solids, two fluid flows, etc. Two models of surface roughening have attracted much attention due to their apparent simplicity and very rich nonlinear phenomenology. One is the Kardar–Parisi–Zhang (KPZ) model [1] which contains a random forcing,

$$\frac{\partial h(x, t)}{\partial t} = \lambda |\nabla h|^2 + \nu_0 \nabla^2 h + \eta(x, t) \tag{1}$$

where $h(x, t)$ is the height of a growing interface and η is a white, Gaussian, random noise which satisfies

$$\langle \eta(x_1, t_1) \eta(x_2, t_2) \rangle = 2 T \nu_0 \delta(x_1 - x_2) \delta(t_1 - t_2). \tag{2}$$

Note that T here is a coefficient not related to the temperature but designated by the same letter since formally it plays the same role.

The second is the Kuramoto–Sivashinsky equation [2,3] which is completely deterministic:

$$\frac{\partial h(x, t)}{\partial t} = \lambda |\nabla h|^2 + \nu_0 \nabla^2 h - \mu \nabla^4 h. \tag{3}$$

The parameter ν_0 is positive in (1) and (2), and negative in (3). The other crucial parameter, λ, measures the strength of the nonlinear interaction. In both models x denotes a point in d-dimensional space. The growth of the interface is discussed in $d + 1$ dimensions. From the point of view of physics the most relevant cases are, of course, $d = 1, 2$.

The KPZ equation was derived as a continuum limit of models describing random particle additions to a growing interface [4]. Without the random force η the fate of $h(x, t)$ is to decay to zero and stay there forever. The KS equation was derived in the context of intrinsic instabilities, like flame propagation. It is linearly unstable, and nonlinearly chaotic, with bounded solutions roaming on a strange attractor forever [5].

Note that in terms of a 'velocity' field

$$v(x, t) = -\nabla h(x, t) \tag{4}$$

the KPZ equation turns into the noisy Burgers (NB) equation

$$\frac{\partial v(x, t)}{\partial t} = -2\lambda (v \cdot \nabla) v + \nu_0 \nabla^2 v - \nabla \eta(x, t). \tag{5}$$

The representation of the KPZ equation is formally reminiscent of the incompressible Navier–Stokes equation. The important difference between these equations is that in the NB equation v is potential, whereas in the Navier–Stokes equation it is solenoidal. We shall use the representation (5) extensively in this paper.

1.2. Overview of previous results in 1+1 dimensions

Our analysis comes in the wake of a number of important studies of the solutions of the KPZ equation (1) in 1+1 dimensions. We shall begin therefore with a short review of the previous results, in order to clarify what is missing and what we propose to accomplish here.

One early important result pertains to the statistics of the solutions of (1). It was proved that the distribution function of the simultaneous double correlators is Gaussian [6]. The irreducible correlation functions of higher orders vanish. Therefore all simultaneous correlators can be factored into products of double correlators

$$n(x) = \langle h(x, t) h(0, t) \rangle. \tag{6}$$

Here the angular brackets mean an average with respect to realizations of the random noise η.

Furthermore, the explicit expression for the correlation function is known [6]. It is convenient to deal with the Fourier representation of the function $n(x)$,

$$n(k) = \int dx\, n(x) \exp(-ikx) \tag{7}$$

which is equal to

$$n(k) = T/k^2. \tag{8}$$

This expression corresponds to the conventional solution in thermodynamic equilibrium with temperature T and energy

$$E = \frac{1}{2} \int v^2(x, t)\, dx = \frac{1}{2} \int |\nabla h(x, t)|^2\, dx. \tag{9}$$

This result is surprising since the KPZ equation describes a non-equilibrium situation. The two reasons for this behaviour are: (i) in 1+1 dimensions and at $\nu_0 = 0$, $\eta = 0$ the KPZ equation conserves the energy E of the system; (ii) the dissipative term with coefficient ν_0 in (1) and the noise η satisfy the Langevin relation (2) and consequently describe the interaction of a system possessing the energy (9) with a thermal bath at 'temperature' T. Consequently this system has to relax to 'thermodynamic equilibrium' with an equipartition of energy over all degrees of freedom.

Let us now consider the Fourier representation $n(k, \omega)$ of the two-time correlator of the field h. The correlator obviously satisfies:

$$n(k) = \int n(k, \omega) \frac{d\omega}{2\pi}. \tag{10}$$

The dependence of the correlator $n(k, \omega)$ on ω can be different for small and large k. For large enough k, the interaction term in (1) becomes irrelevant compared to the dissipative (diffusive) term. How large k should be can be found from comparing these two terms: $\lambda h(x) \simeq \nu_0$. Using (8) we find

$$h^2(x) \simeq \langle h^2(x) \rangle \simeq \int dk\, n(k) \simeq T/k \tag{11}$$

and finally

$$k_* \simeq \lambda^2 T/\nu_0^2. \tag{12}$$

Thus for $k \gg k_*$ we expect the bare value of the correlation function with the dynamical exponent $z = 2$, but for $k \ll k_*$ the solution may have another form.

The existence of a full scaling solution including temporal properties in the region $k \ll k_*$ is widely discussed in the literature. The scaling solution for $n(k, \omega)$ can be represented as

$$n(k, \omega) = \frac{n}{\nu k^{y+z}} \phi\left(\frac{\omega}{\nu k^z}\right) \tag{13}$$

with y and z being the static and dynamic exponents, respectively. ν is some dimensional factor chosen such that νk^z has the units of frequency. This scaling solution of KPZ was examined in the one-loop approximation [7]. Within this approximation a scaling relation was found in the small k limit ($k \ll k_*$), reading

$$2z + y = 5. \tag{14}$$

Using the exact result $y = 2$ following from (10) and (8), one deduces the non-trivial consequence $z = 3/2$.

1.3. Remaining problems and new results

In order to understand whether the scale invariant solution indeed holds, one needs *to examine higher order terms* beyond the one-loop approximation. In doing so, one needs to know how the vertex is renormalized by higher order corrections. It has been shown that, due to the Galilean invariance of (1), the dressed vertex has the *same* scaling exponent as the bare vertex. Thus if *one assumes that the scale invariant solution does exist*, the scaling relation (14) holds to all orders, and $z = 3/2$ becomes an exact result.

But the existence of such a solution needs a proof. The problem is that an examination of the higher order diagrams shows immediately that they suffer logarithmic divergences. The divergences may drastically change the character of the solution and, in particular, may destroy the scaling. Hence methods suitable to take into account the higher order contributions must be used.

Renormalization group (RG) analysis is a well-known method of this type. We shall explain in detail in section 2.3 that RG methods are not applicable to the investigation of the large-scale behaviour of solutions of the KPZ equation in 1+1 dimensions, since the system exhibits 'strong coupling' at large scales. Hence we are compelled to search for other techniques. We shall use a functional integral approach to the Wyld diagrammatic technique, and demonstrate that the KPZ equation has some wonderful properties in 1+1 dimensions. These enable us to establish the character of the solution for the correlation functions. In fact, we shall demonstrate how to control the divergences of the diagrams order by order. We shall show that the divergences cancel exactly between the diagrams of each order. Consequently a scale invariant formulation indeed becomes available, with $z = 3/2$ being the correct result. It is noteworthy that analogous cancellations occur in the perturbation theory for fully developed turbulence [8].

Finally, we consider the relation between KPZ and KS. It has been argued before [9, 10] that for small k these two equations have the same scaling solutions in 1+1 dimensions. Unfortunately, the theoretical assertion [9] was based on shaky ground, since the KS equation was treated with perturbation theory around the unstable propagator. In section 5 we therefore offer the proper theory that leads to the correct conclusion, that indeed the scaling solution of the two equations is the same. The main condition for this conclusion is the 'locality of interaction' in k-space, which is proved in section 5. We stress that this conclusion is *not* true in 2+1 dimensions, where KS may have a different solution due to non-local interactions in k-space [11]. In section 6 we present some analytical results for the scaling function. We evaluate the asymptotic form of the double correlator $n(k, \omega)$ for large frequencies and find that it is proportional to $\omega^{-7/3}$. This form is utilized in section 7 to compare with the numerical simulations.

Section 7 is dedicated to the numerical simulations of KS. We integrate KS for long enough time so that the width is saturated in the mean. After saturation we simulate further, and compute the two-point dynamical correlation functions. These are Fourier transformed and fitted to scaling functions in order to extract the dynamical scaling exponent z. We find that $z = 1.55 \pm 0.06$. In addition we check numerically that the stationary statistics are indeed Gaussian.

Section 8 provides a summary and a discussion of this paper.

2. Diagrammatic approach to KPZ and KS equations

2.1. General remarks

In the region of strong interaction $k \ll k_*$ (cf (12)) it is not a good idea to develop a

perturbation analysis for the KS or KPZ equations around the bare propagators. For KS such an analysis [9] would be meaningless; the linear part of this equation is unstable, and such a perturbation theory is bound to have uncontrolled divergences. For KPZ the dressed Green function is expected to change significantly compared to its bare counterpart, and therefore it would be much better to develop a perturbation treatment around the *renormalized* rather than the bare propagators.

The natural scheme to do so is the diagrammatic technique of the type first suggested by Wyld [12], who investigated hydrodynamic turbulence. This technique was later generalized by Martin *et al* [13], who demonstrated that it may be used for investigating the fluctuation effects in the low-frequency dynamics of any condensed matter system, fluid or not. Then Zakharov and L'vov [14] extended the Wyld technique to the statistical description of Hamiltonian nonlinear-wave fields. In fact this technique is also a classical limit of the Keldysh technique [15], which is applicable to any physical system described by interacting Fermi and Bose fields.

The natural objects in the Wyld diagrammatic technique are the dressed propagators which are the Green function $G(x, t)$ and the double correlator $m(x, t)$. The Green function is defined as the average response of the 'velocity' field (4) to a vanishingly small external 'force' $\delta f(x, t)$ which would be added to the right-hand side of the equation of motion (5)

$$iG(x, t) = \left\langle \frac{\delta v(x, t)}{\delta f(0, 0)} \right\rangle. \tag{15}$$

As a consequence of the causality principle the function $G(t)$ has to be zero for $t < 0$. The double correlator is the correlation function of the 'velocity' field v

$$m(x, t) = \langle v(x, t)\, v(0, 0) \rangle. \tag{16}$$

Assuming stationarity in time and homogeneity in space of the state under consideration it is useful to pass into a k, ω-representation:

$$G(k, \omega) = \int dt\, dx \exp(i\omega t - ikx)G(x, t). \tag{17}$$

Since $G(t) = 0$ for $t < 0$ the function $G(\omega)$ is analytic in the upper half-plane. The analogous representation for the double correlator is

$$m(k, \omega) = \int dt\, dx \exp(i\omega t - ikx)m(x, t). \tag{18}$$

Using the Wyld technique one may derive [12, 14] a system of equations for the dressed propagators, known as the Dyson–Wyld equations:

$$G(k, \omega) = \frac{1}{\omega + i\gamma(k) - \Sigma(k, \omega)} \tag{19}$$

$$m(k, \omega) = |G(k, \omega)|^2 \left[D(k, \omega) + \Phi(k, \omega) \right]. \tag{20}$$

In these equations $\gamma(k)$ is the bare 'damping' (which is $\nu_0 k^2$ for KPZ and $\nu_0 k^2 + \mu k^4$ for KS) and D is the correlator of the external force ($2T\nu_0$ for KPZ and zero for KS). The mass operators $\Sigma(k, \omega)$ and $\Phi(k, \omega)$ are the *self-energy* and *intrinsic noise functions*, respectively. These are given by infinite series of one-particle irreducible diagrams:

$$\Sigma = \Sigma_2 + \Sigma_4 + \Sigma_6 + \dots \qquad \Phi = \Phi_2 + \Phi_4 + \Phi_6 + \dots. \tag{21}$$

In these expressions Σ_{2j} is a functional of $2j$ vertices λ, j double correlators m and $(2j-1)$ Green functions G; Φ_{2j} is a functional of $2j$ vertices λ, $(j+1)$ correlators m and $2(j-1)$ functions G.

To reproduce the perturbation series in compact form it is convenient to use graphic notation for the objects appearing in the expansion, shown in figure 1. A wavy line describes the field v, a straight line is $\delta/\delta f$. In accordance with (15) the Green function G has one wavy section and one straight section, while the double correlator has two wavy sections. There is only one type of vertex Γ, which is the junction of one straight and two wavy lines. The momentum and frequency conservation laws $k = k_1 + k_2$ and $\omega = \omega_1 + \omega_2$ are implied. For convenience we use the wave vectors only to label the diagrams. The topological properties of the diagrams are automatically specified by the junction rules which are formulated on the basis of notation in figure 1. These properties and the rules of 'reading' diagrams are given, for example, in [12, 14].
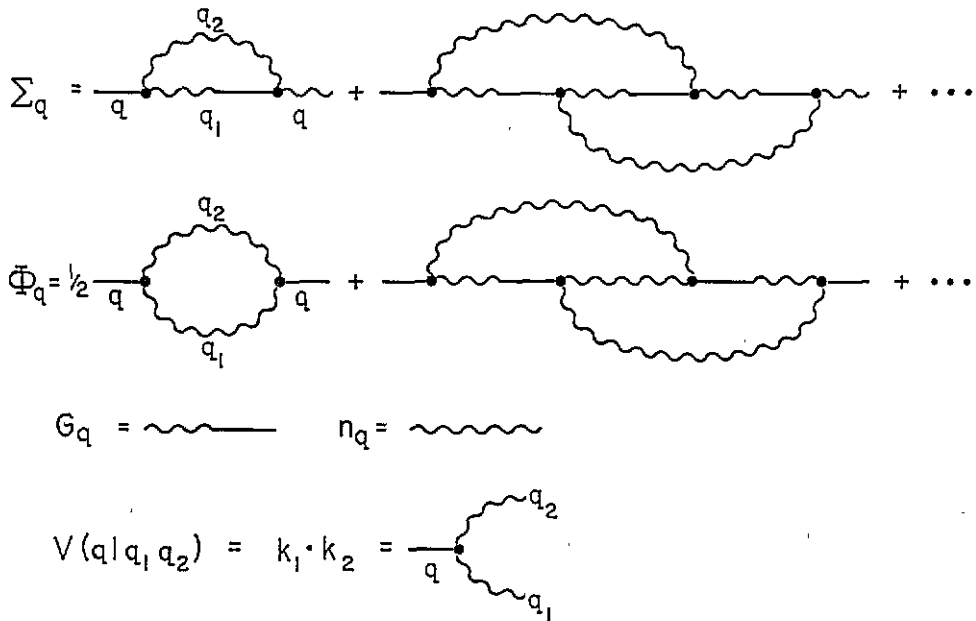

Figure 1. Graphic notation and the lowest order diagrams for the self-energy functions.

Finally, let us prove a useful *sum rule for the dressed Green function*

$$\int d\omega \, G(k, \omega) = -i\pi \tag{22}$$

which follows from the analyticity of $G(\omega)$ in the upper half-plane. The idea of the proof is to deform the contour C_1 of the integration over ω in the upper half-plane. If the contour C_2 goes far enough from the origin (see figure 2) one can neglect $\gamma(k)$ and Σ in equation (19), leading to the asymptotic form $G(\omega) \approx \omega^{-1}$ on the contour. The result (22) follows immediately when the radius of C_2 goes to infinity.
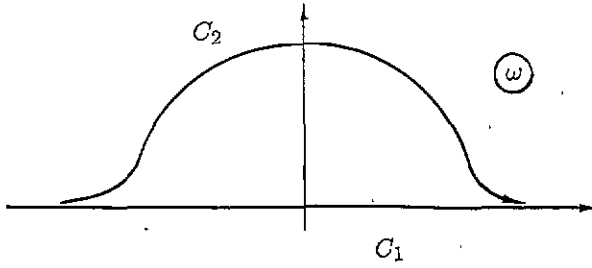
Figure 2. The deformation of the contour of integration over frequency in the complex frequency plane.

The analogous expression to (13) for the Green function in the region of strong fluctuations, $k \ll k_*$, is

$$G(k, \omega) = \frac{1}{\nu k^z} \, g\left(\frac{\omega}{\nu k^z}\right). \tag{23}$$

There is only one scaling exponent in the expression (23) (i.e. the same exponent z appearing twice) because of the relation (22). The condition for the validity of (23) is

$$\int_{-\infty}^{+\infty} d\xi \, g(\xi) = -i\pi. \tag{24}$$

The convergence of the integral in the region of strong interaction, $k \ll k_*$, will be proved later.

The scaling solution for the double correlator has the form

$$m(k, \omega) = \frac{T}{\nu k^z} \, f\left(\frac{\omega}{\nu k^z}\right). \tag{25}$$

The form is compatible with the exact relation (8) if

$$\int_{-\infty}^{+\infty} d\xi \, f(\xi) = 2\pi. \tag{26}$$

2.2. Direct interaction (or one-loop) approximation

Let us consider the lowest order contributions to the self-energy functions Σ and Φ, known also as self-consistent mode-coupling theory [16]. In diagrammatic language they are shown in figure 1(*b*), and the analytical expressions are

$$\Phi_2(k, \omega) = \frac{\lambda^2 k^2}{2} \int \frac{dq \, d\psi}{(2\pi)^2} \, m(q, \psi) \, m(k+q, \omega+\psi) \tag{27}$$

$$\Sigma_2(k, \omega) = \lambda^2 k \int \frac{dq \, d\psi}{(2\pi)^2} \, q \, G(q, \psi) \, m(k-q, \omega-\psi). \tag{28}$$

Substitute the propagators G and m in the scaling forms (23) and (25) into (28). If $z = 3/2$, and if the integral converges, then for $\omega \simeq \nu k^z$

$$\Sigma \simeq \frac{\lambda^2 T k^{3/2}}{\nu}. \tag{29}$$

Since $k^{3/2} > \gamma(k) \simeq k^2$ for small k, in order for G to scale according to (23) with $z = 3/2$, Σ must have an exponent 3/2. Therefore

$$\Sigma \simeq \nu k^{3/2} \simeq \omega \qquad (30)$$

and comparing the two expressions for Σ the value of ν can be estimated as

$$\nu \simeq \lambda\sqrt{T}. \qquad (31)$$

It may be easily checked that all the higher order terms of the perturbation series have the same dimensional estimate. Therefore the solution (23) with $z = 3/2$ seems self-consistent. However, note that simple power counting would predict that the integral diverges. Since the higher order terms have the same dimensional estimate, they suffer logarithmic divergences, because they have loops whose integrals $\sim k^0$. Since the integrand is odd in q for large q (so that $k+q \approx q$), in the one-loop approximation the ultraviolet contributions must cancel. Unfortunately, the fact of ultraviolet cancelations cannot be trivially translated to the higher order diagrams.

In general, the self-consistent procedure is potentially very dangerous. For example, if we applied an analogous procedure to the Landau ϕ^4-model of second-order phase transitions we would obtain an incorrect result. Namely, if we determined self-consistently the exponent η of the anomalous dimension of the double correlator using the diagram depicted in figure 3(a) we would find that η equals 1/2 (in three dimensions), in contradiction with the real value which is close to zero. The problem is that the substitution of the solution with $\eta = 1/2$ for the Green function into the expressions of the perturbation series for the self-energy function (which is depicted in figure 3(b)) gives rise to logarithmic ultraviolet divergences in all the terms. The resummation of the logarithms will change the degree of the self-energy function, destroying the self-consistency [17].
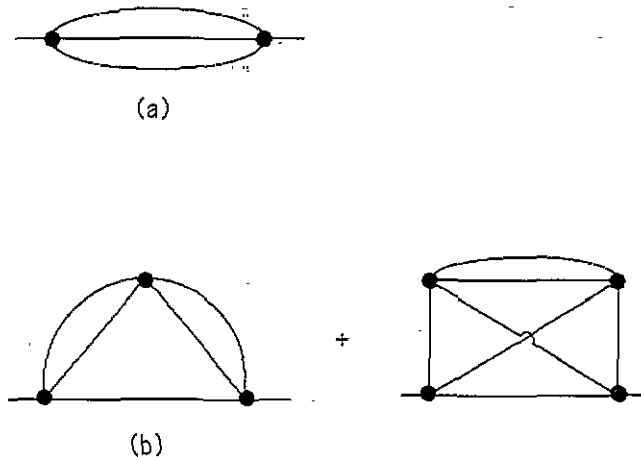

(a)

(b)

Figure 3. The lowest order diagrams for the mass operator (a) and the vertex (b) in the ϕ^4 theory.

The conclusion is that the self-consistent procedure is correct and may be applied for proving scaling only if the ultraviolet divergent terms are absent in the perturbation series for Σ. We shall demonstrate below that the function (23) with the index $z = 3/2$ is indeed the proper scaling solution, since all the divergences cancel!

2.3. *Logarithmic divergences in the vertex and their cancellation*

We have seen that the integral in the expression for Σ_2 converges. In fact, the integral in the expression for Φ_2 converges as well. Let us now consider the two-loop corrections to Σ. The diagrams corresponding to these terms will contain blocks representing one-loop corrections to the vertex shown in figure 4. The analytical expression for the one-loop correction to the vertex is

$$
\begin{aligned}
\Gamma_3(k, \omega | k_1, \omega_1, k_2, \omega_2) = \frac{\lambda^3 k}{(2\pi)^2} k \int dq\, d\psi [&q(q - k_2)G(q, \psi)m(k - q, \omega - \psi) \\
&\times G(q - k_2, \psi - \omega_2) + \tfrac{1}{2}q(k - q)G(q, \psi) \\
&\times G(k - q, \omega - \psi)m(q - k_2, \psi - \omega_2)].
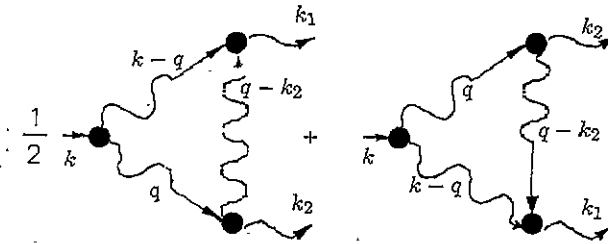\end{aligned}
\tag{32}
$$

Figure 4. *The one-loop corrections to the vertex.*

By substituting the scaling form of the propagators (23) and (25) into (32) one can easily find that this integral diverges logarithmically. When one substitutes the scaling forms with $z = 3/2$, one gets $\Gamma \sim k$, which implies that the integral itself scales $\sim k^0$. This is possible only if the integral is essentially $\int dq/q = \log q$, which diverges in the IR and the UV.

In the following we shall use the important exact relation

$$
m(k, \omega) = iT[G(k, \omega) + G(-k, -\omega)] = -2T\mathrm{Im}G(k, \omega). \tag{33}
$$

This type of relation between the Green function and the double correlator is known as the *fluctuation–dissipation theorem* (FDT), and it follows as a consequence of the 'thermodynamic equilibrium' in this system. It is easy to check the validity of the FDT explicitly in the one-loop order (27) and (28). The general proof of the FDT for the entire diagrammatic series is not so simple. We will prove it later by using a generating functional approach.

After substituting the FDT into (32) one finds that some terms vanish due to the analytical properties of the Green functions. Explicitly, the integral

$$
\int dq\, d\psi\; G(q, \psi)\; G(q - k, \psi - \omega)\; G(q - k_2, \psi - \omega_2)
$$

is equal to zero, since all the functions $G(\psi)$, $G(\psi - \omega)$ and $G(\psi - \omega_2)$ are analytical in ψ in the upper half-plane. Therefore the contour of integration over ψ may be deformed to go arbitrarily far from the origin, as is shown in figure 2. Since the product $G(q, \psi)\, G(q - k, \psi - \omega)\, G(q - k_2, \psi - \omega_2)$ behaves as ψ^{-3} at large ψ, the value of the

contour integral tends to zero for a semicircle of large radius. Consequently the original integral is zero.

After avoiding the vanishing contributions the value of Γ_3 becomes

$$
\begin{aligned}
\Gamma_3(k, \omega | k_1, \omega_1, k_2, \omega_2) = & \frac{i\lambda^3 k\ T}{(2\pi)^2} \int dq\, d\psi [q(q - k_2) G(q, \psi) \\
& \times G(k - q, \omega - \psi) G(q - k_2, \psi - \omega_2) \\
& + \frac{1}{2} q(k - q) G(q, \psi) G(k - q, \omega - \psi) \\
& \times [G(q - k_2, \psi - \omega_2) + G(k_2 - q, \omega_2 - \psi)]].
\end{aligned}
$$

Formally this integral diverges logarithmically (for the same reason that (32) diverges logarithmically). Actually the divergence is cancelled since for large q and ψ we have

$$
\begin{aligned}
\Gamma_3(k, \omega | k_1, \omega_1, k_2, \omega_2) = & i(2\pi)^{-2} \lambda^3 k\ T \int dq\, d\psi\ q^2 G(q, \psi) G(-q, -\psi) \\
& \times [G(q, \psi) - G(-q, -\psi)]
\end{aligned}
$$

which is odd in (q, ψ).

We thus conclude that the analysis of the one-loop diagrams shows that the ultraviolet divergences do cancel in this technique. However, the analysis of higher order diagrams is more cumbersome, and cannot be performed in the same way. Accordingly we have to find another way of exploring the higher order diagrams. In the next section we examine whether renormalization group techniques can solve this issue and find that they cannot.

2.4. Remarks on the RG approach to problems with strong interaction

The problem we encounter is known as the problem of 'strong interaction' of fluctuations. Systems of this kind can exhibit two possible behaviours, in the limit of increasing scale. If the coupling constant decreases, then the system has 'weak coupling', whereas if the coupling constant increases, then the system has 'strong coupling'.

Quantum electrodynamics (QED), whose theory has been examined in detail, is a case of weak coupling, where it is known as the 'zero-charge' problem. In this case, perturbation theory may be safely applied to study the correlation functions at large scales, due to the smallness of the coupling constant. The calculation of correlation functions is reduced to the summation of the principal perturbation sequences, which lead to screened interactions.

The renormalization group (RG) is a very powerful method of accomplishing this. Indeed, RG methods were first developed in the context of QED. They were later widely applied in quantum field theory and in the context of critical phenomena following Wilson's ϵ-expansion method [18]. In particular, RG methods enable one to establish the presence of scaling behaviour of systems in the case of weak coupling (e.g. systems in the vicinity of second-order phase transitions).

Quantum chromodynamics (QCD) is a case of strong coupling, where it is known as 'asymptotic freedom'. The short-distance properties of these systems may be examined by perturbation theory. In the framework of QCD RG methods may be applied to study the correlation functions only in the short-distance regime. In the region of large scales RG methods are not applicable because the coupling constant is of the order unity. As a consequence QCD in this region is still an unsolved problem.

A good example that scaling properties can be destroyed in strong coupling regimes has been provided by exactly solvable models. Two such models are the two-dimensional

SU(N) main chiral field and the n-field which were solved by Wiegmann [19, 20]. In these examples one finds a spontaneous gap appearing in the system, while the Goldstone theorem would have predicted gapless excitations. An analogous behaviour is suggested for QCD.

One of the most intriguing properties of the systems described by KPZ and KS is that they have strong coupling behaviour. It was demonstrated by Forster *et al* [7] that in 2+1 dimensions the coupling constant of the Burgers equation (which is equivalent to KPZ or KS) diverges logarithmically at large scales. Therefore for $d < 2$ the system is strong coupling. This would be also true, of course, for KPZ in 1+1 dimensions.

In conclusion of this subsection we note the work by Medina *et al* [21] who investigated KPZ in the framework of RG and concluded that in 1+1 dimensions there exists an effective weak coupling situation. We would like to stress that their arguments are open to criticism. The problem is that they used the one-loop approximation for the RG equations, although many-loop terms produce contributions to the RG equation which are of the same order as the one-loop term. Thus the assertion of these authors concerning the existence of a fixed point is uncontrolled. We believe that these difficulties rule out RG as an effective theory of KPZ in 1+1 dimensions.

3. Generating functional approach for KPZ

In this section we use functional integration techniques to generate alternative perturbation expansions to the one used in section 2. In particular, we shall use the freedom to change variables in the functional integral in order to achieve different resummations of the perturbation expansion. We shall find a particularly useful resummation in which only Green functions appear but correlators do not. The superior analytic properties of the Green functions will allow us to prove that the perturbation series is free of divergences order by order. A device which is used decisively in our formalism is the fluctuation–dissipation theorem (FDT) which is also proved in this section. We shall assume familiarity with the technique of functional integration, which in this context originates in the well-known ideas of Feynman [22]. A textbook description of functional integration methods closely related to the present problem may be found in the book by Popov [23].

3.1. Relation with the diagrammatic technique

In this subsection we explain the relation between the original Wyld expansion and the functional integral representation of the propagators. The representation of correlation functions appearing in the Wyld technique in the form of functional integrals was first developed by de Dominicis [24] and Janssen [25]. Following the work of de Dominicis and Peliti [26] we may assert that the correlation function of the solutions of equation (1) are generated by the following functional:

$$Z(b, \hat{b}) = \int Dh \, D\hat{h} \, \exp\left(iA + \int dt \, dx(bh + \hat{b}\hat{h})\right). \tag{34}$$

Here $\hat{h}$ is the auxiliary field conjugate to h and the effective action A is

$$A = \int dt \, dx(\hat{h}\partial h/\partial t - \hat{h}\lambda(\nabla h)^2 - \nu_0\hat{h}\nabla^2 h + iT\nu_0\hat{h}^2). \tag{35}$$

The integration in (34) is performed over all functions $h(x, t)$ and $\hat{h}(x, t)$. The variables $b(x, t)$ and $\hat{b}(x, t)$ are arbitrary functions of time t and coordinate x. The coefficients of

the expansion of Z in $b(x, t)$ and $\hat{b}(x, t)$ are the correlation functions of the fields $h(x, t)$ and $\hat{h}(x, t)$.

Note that in the expression of reference [26] there appeared a functional determinant which may be represented in the form of an integral over auxiliary Fermi fields [27, 28]. It can be demonstrated that in the present case the determinant is equal to unity because of the causality properties of the Green functions. Therefore we shall omit the determinant.

The first term in the expansion of Z in $b(x, t)$ and $\hat{b}(x, t)$ has the following form:

$$
\begin{aligned}
Z^{(2)} = \int dt_1 \, dx_1 \, dt_2 \, dx_2 (\tfrac{1}{2} b(x_1, t_1) \langle h(x_1, t_1) \, h(x_2, t_2) \rangle b(x_2, t_2) \\
+ b(x_1, t_1) \langle h(x_1, t_1) \, \hat{h}(x_2, t_2) \rangle \hat{b}(x_2, t_2))
\end{aligned}
\tag{36}
$$

where the brackets $\langle \rangle$ mean an average with weight $\exp(iA)$. The average of h, $\langle h \rangle$, can be taken to equal zero, because the equation of motion is invariant under the transformation $h \longrightarrow h + H$ where H is a constant. $\langle h \, h \rangle$ is the double correlator of the quantity h, whereas $-i\langle h \, \hat{h} \rangle$ is the Green function of the system $\langle \delta h / \delta f \rangle$. Indeed, if an additional external force η_{ext} were added to the right-hand side of equation (1), the effective action A would have a new term $-\eta_{\text{ext}} \hat{h}$. Accordingly, then $\langle h \rangle$ would be

$$
\langle h(x_1, t_1) \rangle = -i \int dt_2 \, dx_2 \langle h(x_1, t_1) \, \hat{h}(x_2, t_2) \rangle \eta_{\text{ext}}(x_2, t_2).
\tag{37}
$$

The causality principle now dictates that

$$
\langle h(x_1, t_1) \, \hat{h}(x_2, t_2) \rangle = 0 \qquad \text{if } t_1 < t_2.
\tag{38}
$$

Note that the correlation function $\langle \hat{h} \, \hat{h} \rangle$ is equal to zero in this technique [26].

When discussing KPZ and KS it is convenient to transform the fields h and $\hat{h}$ into new variables v and p, defined as

$$
v = -\partial h / \partial x \qquad \hat{h} = \partial p / \partial x.
\tag{39}
$$

The effective action A acquires the form $A = A_0 + A_{\text{int}}$ where

$$
A_0 = \int dt \, dx \left[p \frac{\partial v}{\partial t} + v_0 \frac{\partial p}{\partial x} \frac{\partial v}{\partial x} + iT v_0 \left(\frac{\partial p}{\partial x} \right)^2 \right]
\tag{40}
$$

$$
A_{\text{int}} = -\lambda \int dt \, dx \, v^2 \frac{\partial p}{\partial x}.
\tag{41}
$$

A_0 determines the bare values of the correlation functions of v and p, and A_{int} is responsible for the renormalization of the bare values.

Now the Green function (15) and the double correlator (16) may be rewritten in the form of functional integrals:

$$
G(x, t) = \langle v(x, t) \, p(0, 0) \rangle \equiv \int Dp \, Dv \, \exp(iA) \, v(x, t) \, p(0, 0)
\tag{42}
$$

$$
m(x, t) = \langle v(x, t) \, v(0, 0) \rangle \equiv \int Dp \, Dv \, \exp(iA) \, v(x, t) \, v(0, 0).
\tag{43}
$$

The double correlator $\langle p(x, t) \, p(0, 0) \rangle$ is exactly zero and therefore it does not appear in the expansion.

We see now that the graphic notations of figure 1(a) are dictated by (42) and (43) for G and m: a wavy line describes the field v, and a straight line is the field p. In accordance with (42) the Green function G has wavy and straight lines while double correlators of the field v have two wavy lines in accordance with (43). The particular form of the action A_{int}, having a product of one field p (straight line) and two fields v (two wavy lines), leads to only one type of vertex Γ which is the junction of one straight and two wavy lines (see figure 1(a)).

By expanding the functional (34) with respect to the action A_{int} and performing the Gaussian integration, one can reproduce the perturbation series for the Green function and double correlator described above. The technical details of such a procedure may be found in the book by Popov [23]. We have thus established the connection between the two approaches and are ready to make use of the second formalism.

3.2. Fluctuation–dissipation theorem (FDT)

In this subsection we prove the FDT using the functional integration technique. With this intention let us transform the field p into a new field $\tilde{p}$ which is

$$\tilde{p} = p - iv/2T. \tag{44}$$

The effective action A defined by (40) and (41) acquires the form

$$A = \int dt \, dx \left[\tilde{p} \, \frac{\partial v}{\partial t} + \frac{iv_0}{4T} \left(\frac{\partial v}{\partial x} \right)^2 + iT v_0 \left(\frac{\partial \tilde{p}}{\partial x} \right)^2 - \lambda \, \frac{\partial \tilde{p}}{\partial x} \, v^2 \right]. \tag{45}$$

This action is invariant under the transformation

$$t \longrightarrow -t \qquad v \longrightarrow -v \qquad \tilde{p} \longrightarrow \tilde{p}. \tag{46}$$

Therefore (in the absence of spontaneous breaking of time reversal) the correlation function $\langle v \, \tilde{p} \rangle$ must change its sign at $t \longrightarrow -t$, i.e.

$$\langle v(t) \, \tilde{p}(0) \rangle = -\langle v(-t) \, \tilde{p}(0) \rangle.$$

In addition, both KPZ and KS are invariant under the transformation $x \longrightarrow -x$, so their solutions have this symmetry as well, and we can write

$$\langle v(x, t) \, \tilde{p}(0, 0) \rangle = -\langle v(-x, -t) \, \tilde{p}(0, 0) \rangle.$$

Performing the Fourier transformation and bearing in mind the definitions (42), (43) and (44) we derive the FDT equation (33).

4. Divergences in higher order diagrams and a proof of their cancellation

At this point we shall obtain the central result of this paper, i.e. the cancellation of ultraviolet divergences in the perturbation expansion. For this purpose we shall use yet another change of variables in the functional integral to achieve a perturbation theory in terms of only one type of propagator, namely the Green function. This rearrangement of the perturbation theory is possible due to the existence of the FDT. The fact that only Green functions appear will enable us to use their analytical properties to prove the cancellation of all divergences order by order.

4.1. A rearrangement of the perturbation theory

To construct the rearranged diagrammatic series we introduce the new field $\tilde{v}$:

$$\tilde{v} = v + iTp. \tag{47}$$

The series will be constructed in terms of the fields p and $\tilde{v}$. As a consequence of the FDT (33) and the fact that $\langle p\, p \rangle = 0$ we see that $\langle \tilde{v}\, \tilde{v} \rangle = 0$, whereas the new Green function

$$\langle \tilde{v}(x,t)\, p(0,0) \rangle = G(x,t) \tag{48}$$

is exactly the same Green function (42) as before! This is the advantage of the new construction: only Green functions, with simple analytical properties, appear in the perturbation series.

The Dyson equation (19) will obviously have the same form in the new variables $\tilde{v}$ and p. To formulate the diagram rules for computing Σ directly in these variables we must rewrite the effective action A in terms of $\tilde{v}$ and p. The result is

$$A = \int dt\, dx \left[p\, \frac{\partial \tilde{v}}{\partial t} + v_0\, \frac{\partial p}{\partial x}\, \frac{\partial \tilde{v}}{\partial x} - \lambda \left(\frac{\partial p}{\partial x}\, \tilde{v}^2 + iT\, \frac{\partial \tilde{v}}{\partial x}\, p^2 \right) \right]. \tag{49}$$

This effective action will produce two types of vertices in the diagrammatic expansion. The old vertex λk is still a junction of one p-straight and two v-wavy lines. The new vertex $i\lambda T k$ connects one wavy and two straight lines (see figure 5).
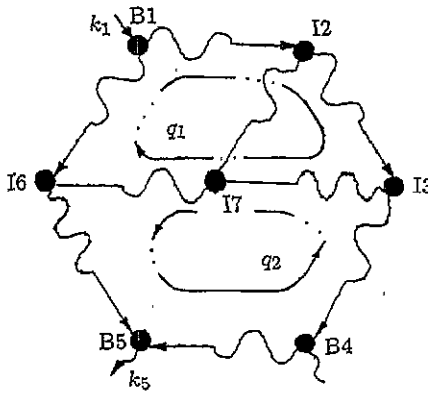

Figure 5. A schematic representation of a typical block in a general diagram. The boundary vertices are denoted by (B) and the internal vertices by (I). Every boundary vertex has a dangling bond that connects this block to other parts of the diagram. A directed path is, for example, the path starting at B1, going through B2–I3–I4 and ending at B5.

4.2. Cancellation of divergences

In this subsection we use the rearranged perturbation series to show that all the divergences cancel. We do this by considering a representative diagram from the series for Σ. The schematic structure of a typical block (substructure) of such a diagram is presented in figure 5. There are a number of vertices which are connected by lines representing Green

functions (48). All the vertices of any block are either internal vertices or boundary vertices. The latter connect the block with other parts of the diagram. An internal vertex (I) always joins three lines whereas a boundary vertex (B) connects two lines belonging to the block.

Let us define a 'directed' path going through the block along lines representing Green functions, in the direction from the wavy segment to the straight segment. Starting such a path at any chosen vertex we can encounter many bifurcation points, but the path can never end in the interior of the block, unless it is a closed loop (the only way that a path could end in the interior is by having a vertex joining three straight segments, but such a vertex does not exist in this theory). Analogously each directed path may be extended in the opposite direction through all interior vertices. See figure 5 for an example.

Thus we conclude that when we consider the entirety of all the 'directed' paths, extended in both directions as long as possible, they can either start and end at a boundary vertex, or consist of a closed loop.

The main point of this exercise is that *all diagrams containing any directed closed loops vanish identically*. The reason is most clearly seen in the t-representation, where a closed loop means an integral

$$\int dt_1 \, dt_2 \ldots dt_n \; G(t_1 - t_2) \, G(t_2 - t_3) \ldots G(t_n - t_1). \tag{50}$$

Due to causality $G(t - s)$ vanishes for $s > t$, and the integral (50) has to vanish as well. Next we examine therefore those blocks which contain no directed closed loops. We shall show that such blocks have *no divergences* in the ultraviolet.

For this purpose consider first a block which includes a loop containing n vertices and n propagators (see figure 5, where $n = 6$ for the loop B1–I2–I3–B4–B5–I6–B1). Suppose in this loop there are two directed paths with opposite directions, one having s vertices ($s = 5$ in figure 5) and the other $n - s + 2$ ($= 3$ in figure 5). In this case there will be two vertices dividing the directed paths (vertices B1 and B5 in figure 5). Let us designate the 'incoming' wave vector through the first vertex (B1 in figure 5) as k_1, and the 'outgoing' wave vector through the second vertex (B5 in figure 5) as k_5.

The loop corresponds to an integral over an 'inner' wave vector q, and we examine in power counting whether for q much larger than both the incoming k_1 and the outgoing k_5 we can have UV divergences.

Every vertex connecting two equally directed links contributes a q factor to the integrand whereas the vertices having the 'incoming' and 'outgoing' wave vectors contribute the factor $k_1 k_5$. Thus, the n vertices contribute $k_1 k_5 q^{n-2}$. The n Green functions contribute $(q^{3/2})^{-n}$ (for $z = 3/2$) and the integration $dq \, d\psi$ contributes $q^{5/2}$. The total power is $q^{1/2-n/2}$, and therefore there is no UV divergence in such a loop. Clearly if there are more inversions of directions in a loop, the integral converges even better.

Next we decorate the loop with an additional bridge, for example I3–I7–I6; see figure 5. Then we generate two loops, the inner wave vectors of which we shall designate as q_1 and q_2, respectively. If any of the subloops is fully directed, the entire contribution vanishes. We have to consider only subloops containing at least one inverted segment. Each subloop converges by itself in the UV, due to the previous argument. The total two-dimensional integral where $q_1 \sim q_2 \gg k_1, k_2$ has the same estimate as the whole loop without the bridge, due to the scaling relation. We thus see that such blocks cannot diverge.

By induction, further decoration of any loop by either more bridges or more inverted links produces diagrams that converge at least as well as the undecorated single loop. So we have ended the proof of the absence of ultraviolet divergent terms in the perturbation series for Σ and therefore may conclude that the Green function G in the region of strong

interaction has the scaling form (23) with $z = 3/2$. The double correlator for the variable v has the scaling form (25) with the same $z = 3/2$ and is related to the Green function in accordance with (33).

5. Relation between KS and KPZ: locality of solutions and universality

The relation between the long-wavelength properties of KS and KPZ has been discussed in previous papers. It is believed that in 1+1 dimensions these equations lead to the same scaling solution in the small wave vector limit. Superficially, these equations seem very different, one having positive viscosity and a random forcing, while the other has negative viscosity and no external forcing at all. These differences indeed cause these two equations to differ in an essential way in 2+1 dimensions [11]. Thus we should explain first why in 1+1 dimensions one could expect KS and KPZ to yield the same scaling solution.

The proof is based on the following points.

(i) The nonlinear interaction is the same in the two equations. Thus if there is a situation in which the nonlinear term is dominant in determining the IR scaling properties, we can expect similarities (see below for further discussion).

(ii) In 1+1 dimensions the estimate (12) shows that for KPZ indeed the nonlinear term becomes crucial for $k \ll k_*$. A similar phenomenon exists in KPZ in 2+1 dimensions, where the fluctuation contributions are essential for

$$k \leqslant k_{**} = \Lambda \ \exp\left(-\frac{v_0^2}{\lambda^2 T}\right)$$

where Λ is a cut-off. For KS the situation is more complicated because of the instability which leads to a considerable role of fluctuations in the whole region of negative bare viscosity. Since there is no conservation law in 2+1 dimensions, the difference stated above can lead to different behaviour of the solutions of these two equations [11].

(iii) It is evident that KS and KPZ have very different solutions in the UV regime. The reason is that the linear terms and the noise are totally different, and they dominate the solutions in the UV by the same argument as in (ii). Thus, if the interaction between distant regions in k-space were essential, then the difference in the UV would have directly reflected itself also in the IR. *Thus the proof of the identity of the IR scaling solution of KS and KPZ requires a proof of the locality of interaction* in k-space.

The locality of interaction results here from two phenomena which are interrelated. The first is the existence of scale invariant solutions in the range $1/L \ll k \ll k_*$, where L is the size of the system. This means that in this range there exist no dimensionless constants except kL and k/k_*. The second is the convergence of the integrals which appear in the diagrams for the propagators $G(k, \omega)$ and $n(k, \omega)$ (or $m(k, \omega)$). Since convergence is proved both in the IR and the UV regimes, the only important contribution to the integrals comes from the region $k/q \sim O(1)$, where q is the variable of integration. Our proof of §4 translates to a proof of the locality of interactions for KS and KPZ in 1+1 dimensions, leading to the identity of their scaling behaviour in this regime of k-space.

6. Properties of the scaling functions

In this section we consider the form of the scaling function, especially in the large-frequency domain. The results are tested in the next section against numerical simulations of KS.

Considering for example the correlator (25), we want to find the asymptotic behaviour for $\omega \gg vk^z$. The scaling function f must decrease to zero in this regime as some power of its argument,

$$m(k, \omega) \sim \frac{T}{vk^z} \left(\frac{vk^z}{\omega} \right)^\alpha \tag{51}$$

where α is an unknown exponent that we want to evaluate. To this end we can use equation (20) in the asymptotic regime, i.e.

$$m(k, \omega) \sim \frac{1}{\omega^2} \Phi(k, \omega) \tag{52}$$

where use has been made of the fact that the Green function $G(k, \omega)$ behaves like ω^{-1} for large frequencies. Thus in order to find α we need to estimate Φ in the asymptotic limit. We start with the lowest order approximation (27), and later consider higher order corrections.

There are two natural possibilities which arise in estimating the integral (27), depending on the region of q which gives the main contribution. If the important region is $q \sim k$ then

$$\Phi_2(1) \approx k^3 \, m(k) \, m(k, \omega) \approx k^3 \, \frac{T^2}{k^z} \left(\frac{vk^z}{\omega} \right)^\alpha. \tag{53}$$

On the other hand, if the important region of integration is $q \sim \omega^{1/z} \gg k$, then

$$\Phi_2(2) \approx k^2 \, q \, m(q) \, m(q, \omega) \approx k^2 \, T^2 \omega^{(1-z)/z}. \tag{54}$$

The ratio of these two estimates is

$$\frac{\Phi_2(1)}{\Phi_2(2)} \approx \left(\frac{k^z}{\omega} \right)^\beta \tag{55}$$

where $\beta = \alpha - 1 + 1/z = \alpha - 1/3$. Since, according to (53) and (54) Φ_2 goes to zero when ω is increasing in any case, we conclude from (52) that $\alpha > 2$. Consequently $\beta > 0$, and the contribution (54) is dominant. Combining (51) and (54) we get finally

$$\alpha = 2 + \frac{(z-1)}{z} = \frac{7}{3}. \tag{56}$$

Upon substituting in (51) we find the interesting result that

$$m(k, \omega) \sim \frac{T^{5/3} \, k^2}{\omega^{7/2}} \tag{57}$$

where we used the estimate (30) for v. We draw the reader's attention to the fact that $n(k, \omega) = m(k, \omega)/k^2 \sim T^{5/3}/\omega^{7/2}$, independent of k in this regime. This result agrees with those found in [16] in the one-loop approximation. Note that the statement in [16] that one-loop approximation is exact for KPZ in 1+1 dimensions with strong coupling is untenable.

7. Numerical simulation of the KS equation in 1+1 dimensions

7.1. Method of computer simulation

The equation for the velocity field associated with the KS equation is solved numerically using real-space integration. The spatial derivatives are discretized using standard forward–backward differences on a linear lattice of L sites spaced Δx apart. Denoting $v(n\Delta x, t)$ by v_n, the following system of first-order ordinary differential equations is obtained:

$$\frac{\partial v_n}{\partial t} = -\frac{\lambda}{\Delta x}\left[v_{n+1}^2 - v_{n-1}^2\right] + \frac{\nu_0}{(\Delta x)^2}\left[v_{n+1} - 2v_n + v_{n-1}\right]$$
$$- \frac{\mu}{(\Delta x)^4}\left[v_{n+2} - 4v_{n+1} + 6v_n - 4v_{n-1} + v_{n-2}\right]. \tag{58}$$

Periodic boundary conditions are imposed on $h(x, t)$ and its derivatives. In particular, this implies that the average of $v(x, t)$ over the length of the system is zero:

$$\int_0^{(L-1)\Delta x} v(x, t)\, dx = 0.$$

The parameters are chosen to be $L = 4096$, $\Delta x = 1$, $\lambda = -\frac{1}{2}$, $\nu_0 = -1$, and $\mu = 1$.

The equations are integrated using the ODEX code of Hairer and Wanner [29]. This is an extrapolation algorithm (GBS) based on the explicit midpoint rule. The version we use has a dense output option which allows the solution to be calculated at any time by interpolation from the solution at the timesteps of integration. The timesteps themselves are adapted by the code to keep the local error of v_n below $10^{-6} \cdot |v_n| + 10^{-6}$. Since $O(v_n) \sim 1$, the local error is kept below 10^{-6}.

The equation is integrated from random initial conditions to $t_s = 75\,000$ to ensure that the width has saturated in the mean. Then the pair correlation function $m(k, \omega)$ is calculated in the following manner.

(i) At times $t_j = t_s + j\tau$, where $\tau = 10$, the solution $v(x_n, t_j)$ is Fourier transformed in space to give $v(k_n, t_j)$, where $k_n = 2\pi n/L$ and n takes integer values from 0 to $L - 1$;

(ii) for each k_n, the set $\{v(k_n, t_j)|j = 1, 2, \ldots, 2048\}$ is Fourier transformed in time to give $v(k_n, \omega_j)$, where $\omega_j = 2\pi j/(2048 \cdot 10)$;

(iii) since the velocity field takes real values, $v(-k, -\omega) = v(k, \omega)^*$ and $m(k_n, \omega_j) = |v(k_n, \omega_j)|^2$;

(iv) this procedure is repeated 40 times, with the final 1024 values of t_j in one set coinciding with the first 1024 values of t_j in the next set, and then the 40 values of each $m(k_n, \omega_j)$ are averaged.

The total time of integration is $t = 284\,920$, which requires 410 hours of CPU time on an IBM Risc System /6000, 320H.

7.2. Results

The results of the numerical simulations will be discussed in terms of spectra, scaling functions and the statistics of the fluctuations. The results for the spectrum are not new [10], except that we have a larger system size L; see figure 6. Indeed, the $1/k^2$ behaviour at small values of k is obvious. The local maximum in the spectrum corresponds to the region of fastest growing linearly unstable modes, having the largest value of $\gamma(k)$.
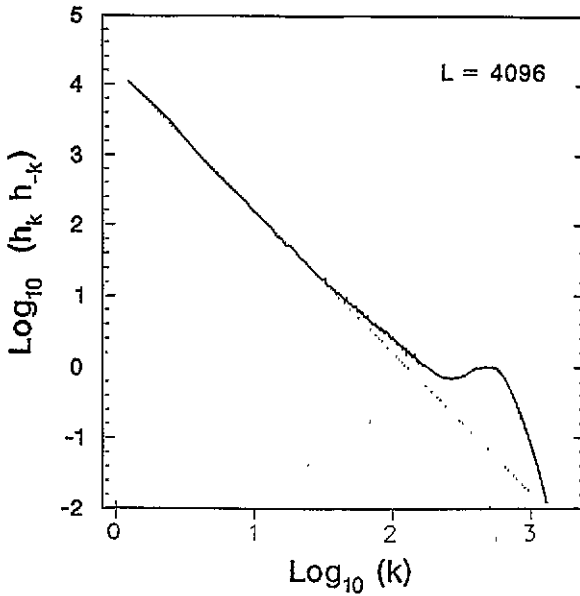
Figure 6. The power spectrum $n(k)$ for a system whose size $L = 4096$ in double logarithmic scale. The local maximum corresponds to the fastest growing linearly unstable modes.

The results for the computed correlation functions $m_{comp}(k, \omega)$ are fitted to a simple functional form

$$m_{tnal}(k, \omega) \equiv \frac{c\omega_k^{\alpha-1}}{(\omega^2 + \omega_k^2)^{\alpha/2}}. \tag{59}$$

Here c is the normalization constant and α is an *a priori* unknown exponent which determines the large-frequency asymptotic. The characteristic frequency ω_k of fluctuations with the wave vector k has to be proportional to k^z where z is a second *a priori* unknown (dynamic) scaling exponent.

The regime of k values for which we expect this form to fit our computed double correlators can be guessed from the spectrum in figure 6. The scaling regime should start at a k value which is a few factors of the inverse system size, and end at a value which is about an order of magnitude smaller than the maximum in the spectrum. We therefore examine the fit in this range of k values. The constant c was determined by us from the condition

$$\int m_{comp}(k, \omega) \, d\omega = \int m_{trial}(k, \omega) \, d\omega. \tag{60}$$

In the following we represent the normalized functions $m_{comp}(k, \omega)$ and $m_{trial}(k, \omega)$ which are divided by c.

In figure 7 we compare the best fit with the value of $\alpha = 2$ to the function (58) with a fit with the value $\alpha = 7/3$, for two representative values of k in the scaling regime, i.e. $k = 12$ and $k = 20$. Clearly, the fit with $\alpha = 7/3$, which is consistent with $z = 3/2$, is superior to the best fit with $\alpha = 2$.
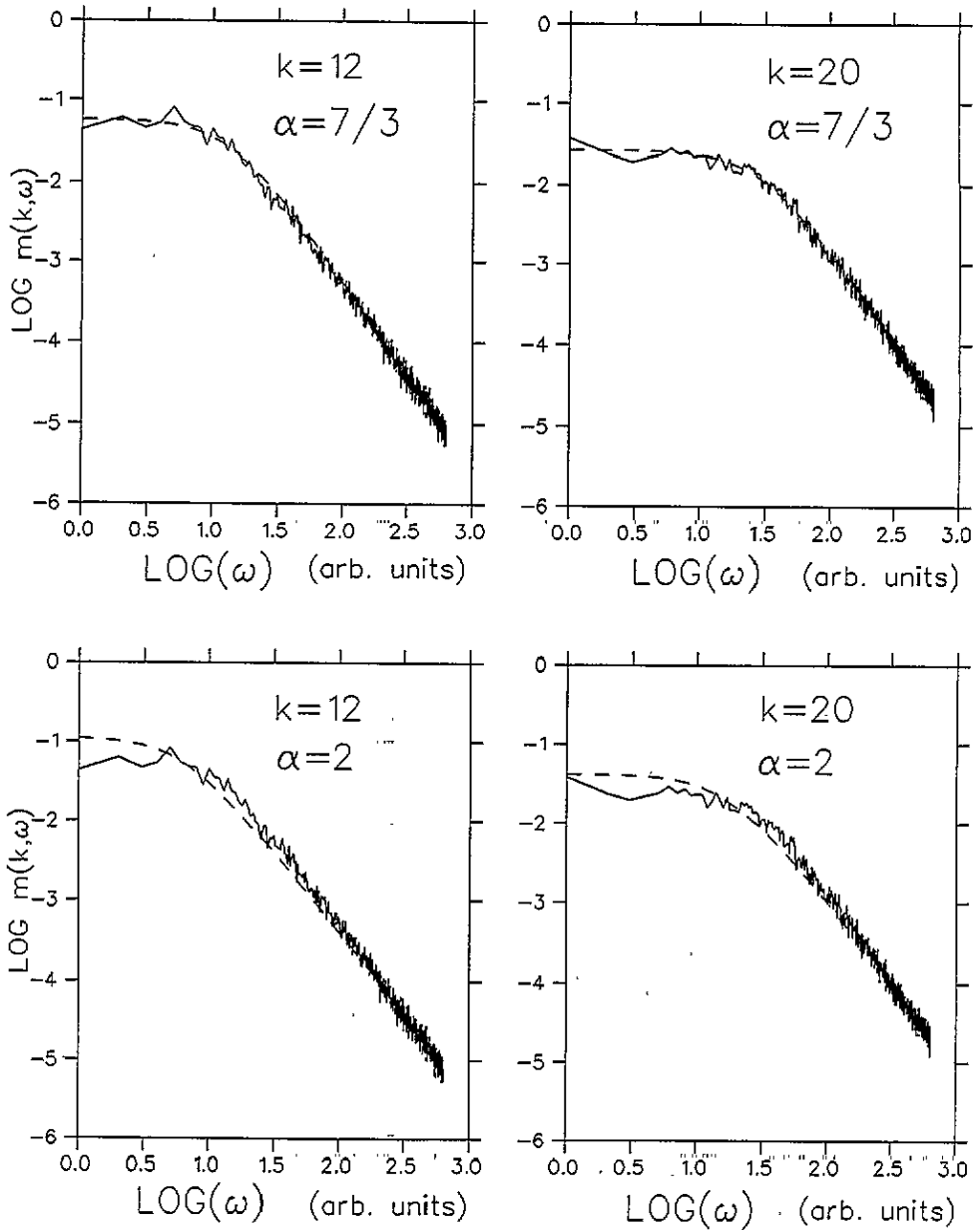
Figure 7. Typical fits of the scaling functions to the numerical data for $\alpha = 7/3$ and $\alpha = 2$ for two values of k in the scaling regime.

To test the quality of the fit to $z = 3/2$ further, we have fitted the scaling function to the double correlators over a wide range of k values, i.e. from $k = 4$ to $k = 64$. In this fit we have chosen $\alpha = 7/3$ and obtained the best value of ω_k. One could use this value directly to find z. However, this value of ω_k is not precise enough for large k, due to the limited region of frequencies. This limited range of frequencies also forced us to normalize the correlators on a subrange of frequencies. Therefore, a better way of evaluating the value of

ω_k for each k is obtained from the value of the fit function at $\omega = 0$. Using these values we show in figure 8 a double logarithmic plot of ω_k against k. The best linear fit yields $z = 1.55 \pm 0.06$, in satisfactory agreement with the theory.
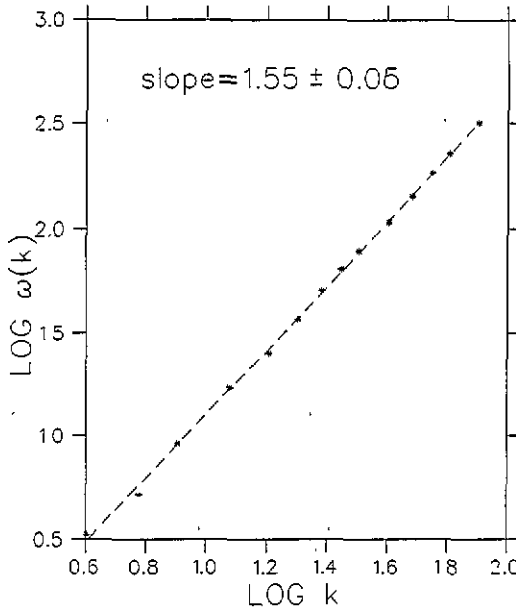

Figure 8. A linear fit of ω_k versus k on a double logarithmic plot. The slope is the value of the dynamical exponent $z \simeq 1.55$.

Finally, we examined the statistics of the fluctuations. In figure 9 we exhibit the logarithm of the probability function of $|h_k|^2$ for a range of k, all normalized by the double correlator, plotted against $|h_k|^2$. The agreement with the expectation of Gaussian behaviour is manifest.

8. Summary and discussion

In summary, we have presented a theory of KPZ and KS in 1+1 dimensions which is valid to all orders in perturbation theory, and which provides the first proof of the validity of the scaling relation (14) and therefore of the result $z = 3/2$. In addition, due to the demonstration of locality of interactions in k-space, we have proved the identity of the scaling behaviour of KS and KPZ in the small-k limit. We reiterate that this identity is special to 1+1 dimensions. In [30] there are arguments that scaling solutions for these two models bifurcate exactly in 2+1 dimensions.

The simulations of KS in 1+1 dimensions support the conclusions of the identity of KS and KPZ at small k. It is noteworthy that the common technique of estimating z from the time-dependent growth of the width of the interface fails altogether for systems of the size used here. The free-field behaviour $z = 2$ is observed, and saturation to the final width sets in before true nonlinear behaviour changes z to its dressed value. The technique used above, of computing the stationary different time correlators, overcomes this difficulty in
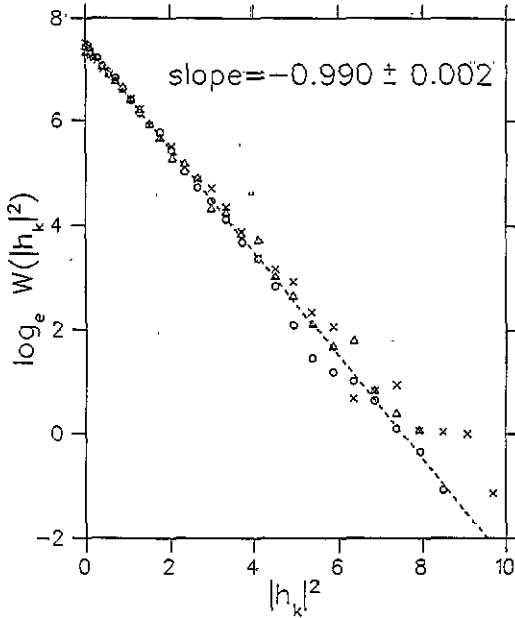
46 *V S L'vov et al*

Figure 9. The probability distribution functions $W\left(|h_k|^2\right)$ vs $|h_k|^2$ in a log-linear scale. The linear fit corresponds to a Gaussian distribution.

a satisfactory manner. The proof of locality can be generalized for $d+1$ dimensions (see [31]).

Some fascinating theoretical issues remain. When and how do the KS and KPZ models bifurcate in their small-k scaling behaviour? How may one find the static exponents in other dimensions? These questions are open to discussion. Their interest stems from the fact that we have here almost tractable examples of strong coupling behaviour that can shed important light on other such systems.

Acknowledgments

VSL acknowledges the Meyerhoff fellowship at the Weizmann Institute of Science. VVL acknowledges the Landau–Weizmann programme. IP acknowledges the partial support of the German–Israeli Foundation and the US–Israel Binational Science Foundation. We thank David Mukamel for interesting discussions and Jean-Pierre Eckmann for his expert advice concerning the KS equation and its numerics.

References

[1] Kardar M, Parisi G and Zhang Y-C 1986 *Phys. Rev. Lett.* **56** 889
[2] Kuramoto Y 1978 *Suppl. Prog. Theor. Phys.* **64** 346
[3] Sivashinsky G 1977 *Acta. Astron.* **4** 1177
[4] Kim J M and Kosterlitz M 1989 *Phys. Rev. Lett.* **62** 2289
[5] Nicolaenko B, Schaurer B and Temam R 1985 *Physica* **16D** 155
[6] Deker U and Haake F 1975 *Phys. Rev.* A **11** 2043
[7] Forster D, Nelson D R and Stephen M J 1977 *Phys. Rev.* A **16** 732

[8] L'vov V S 1991 *Phys. Rep.* **207** 1
[9] Yakhot V 1981 *Phys. Rev.* A **24** 642
[10] Zaleski S 1989 *Physica* **34D** 427
[11] Procaccia I, Jensen M H, L'vov V S, Sneppen K and Zeitak R 1992 *Phys. Rev.* A in press
[12] Wyld H W 1961 *Ann. Phys., NY* **14** 143
[13] Martin P C, Siggia E D and Rose H A 1973 *Phys. Rev.* A **8** 423
[14] Zakharov V E and L'vov V S 1975 *Radiophys. Quantum Electron.* **18** 1084
[15] Keldysh L V 1964 *Zh. Eksp. Teor. Fiz.* **47** 1515 (Engl. transl. 1965 *Sov. Phys.–JETP* **20** 1018)
[16] Hwa T and Frey E 1991 *Phys. Rev.* A **44** R7873
[17] Patashinskii A Z and Pokrovskii V L 1966 *Zh. Eksp. Teor. Fiz.* **50** 439 (Engl. transl. 1966 *Sov. Phys.–JETP* **23** 292)
[18] Wilson K C and Kogut J 1974 *Phys. Rep.* C **12** 76
[19] Wiegmann P B 1984 *Zh. Eksp. Teor. Fiz. Pis. Red.* **39** 180 (Engl. transl. 1984 *Sov. Phys.–JETP Lett.* **39** 214)
[20] Wiegmann P B 1985 *Zh. Eksp. Teor. Fiz. Pis. Red.* **41** 79 (Engl. transl. 1985 *Sov. Phys.–JETP Lett.* **41** 95)
[21] Medina E, Hwa T, Kardar M and Zhang Y-C 1989 *Phys. Rev.* A **39** 3053
[22] Feynman R and Hibbs A R 1965 *Quantum Mechanics and Path Integrals* (New York: McGraw-Hill)
[23] Popov V N 1983 *Functional Integrals in Quantum Field Theory and Statistical Physics* (Dordrecht: Reidel)
[24] de Dominicis C 1976 *J. Physique* C **1** 247
[25] Janssen H K 1976 *Z. Phys.* B **23** 377
[26] de Dominicis C and Peliti L 1978 *Phys. Rev.* B **18** 353
[27] Feigelman M V and Tsvelik A M 1982 *Zh. Eksp. Teor. Fiz.* **83** 1430 (Engl. transl. 1982 *Sov. Phys.–JETP* **56** 823)
[28] Lebedev V V, Sukhorukov A L and Khalatnikov I M 1983 *Zh. Eksp. Teor. Fiz.* **85** 1590 (Engl. transl. 1983 *Sov. Phys.–JETP* **58** 925)
[29] The subroutine used is an extension of the program ODEX described in Section II.9 of Hairer E, Norsett S P and Wanner G 1987 *Solving Ordinary Differential Equations I. Nonstiff problems. Springer Series in Computational Mathematics* vol 8 (Berlin: Springer). The dense output is described in Hairer E and Ostermann A 1989 *Dense output for extrapolation methods. Report* University of Geneva, August
[30] L'vov V and Procaccia I 1992 Comparison of the scale invariant solutions of the KPZ and KS models in $(d + 1)$ dimensions, submitted to *Phys. Rev. Lett.*
[31] L'vov V and Lebedev V 1992 Interactions locality and scaling solutions in the $(d + 1)$ KPZ and KS models, submitted to *Europhys. Lett.*